Accepted Manuscript

Luminescence properties of MOCVD grown $Al_{0.2}Ga_{0.8}N$ layers implanted with Tb

J. Rodrigues, M. Fialho, S. Magalhães, K. Lorenz, E. Alves, T. Monteiro

PII: S0022-2313(18)31844-1

DOI: https://doi.org/10.1016/j.jlumin.2019.02.060

Reference: LUMIN 16326

To appear in: *Journal of Luminescence*

Received Date: 8 October 2018

Revised Date: 26 February 2019

Accepted Date: 28 February 2019

Please cite this article as: J. Rodrigues, M. Fialho, S. Magalhães, K. Lorenz, E. Alves, T. Monteiro, Luminescence properties of MOCVD grown $Al_{0.2}Ga_{0.8}N$ layers implanted with Tb, *Journal of Luminescence* (2019), doi: https://doi.org/10.1016/j.jlumin.2019.02.060.

Luminescence properties of MOCVD grown $Al_{0.2}Ga_{0.8}N$ layers implanted with Tb

J. Rodrigues[1*], M. Fialho[2], S. Magalhães[2], K. Lorenz[2,3], E. Alves[2], T. Monteiro[1]

[1]*Departamento de Física & I3N, Universidade de Aveiro, 3810-193 Aveiro, Portugal*

[2]*IPFN, Campus Tecnológico e Nuclear, Instituto Superior Técnico, Universidade de Lisboa, Estrada Nacional 10, 2695-066 Bobadela LRS, Portugal*

[3]*Instituto de Engenharia de Sistemas de Computadores- Microsistemas e Nanotecnologias (INESC-MN), Rua Alves Redol 9, 1000-029 Lisboa, Portugal*

*Corresponding author: joana.catarina@ua.pt

Keywords: $Al_xGa_{1-x}N$; Tb^{3+}; ion implantation; photoluminescence; yellow luminescence

Abstract

$Al_xGa_{1-x}N$ (x=0.20) layers grown on (0001) sapphire substrates by metal organic chemical vapour deposition were implanted with terbium (Tb) ions at 150 keV with a fluence of 7×10^{14} Tb cm^{-2} at different temperatures. After thermal annealing, all the layers evidenced the Tb-related $^5D_4$-^7F_J intra-4f^8 transitions, demonstrating an enhancement of their intensity with increasing implantation temperature. A detailed spectroscopic analysis of the optical properties of these layers was conducted using luminescence techniques. An atypical behaviour for the relative intensity of both the broad visible bands and the intraionic lines was found as a function of temperature and its origin is discussed based on potential fluctuation phenomena and energy transfer processes. The $^5D_4$-^7F_J intra-4f^8 transitions exhibit thermal population with increasing temperature between ~100 K and ~200 – 230 K, with a subsequent decrease up to RT due to further competitive non-radiative recombination paths. The values calculated for the population energies of each sample are in well agreement with the ones obtained for the activation energies of the de-excitation of the yellow broad band also present in the spectra, suggesting a correspondence between the host defect de-excitation processes and the population of the ion emitting levels.

1. Introduction

III-nitride based semiconductors have been widely used as hosts for the incorporation of luminescent activators, particularly rare earth (RE) ions. Such RE-doped materials constitute auspicious platforms in the optoelectronic field, especially owing to the remarkable atomic-like intra-4f^n transitions exhibited by the trivalent charged ions. These transitions can be extended over all the visible range, depending on the RE ion chosen [1–4].

As evidenced by Favennec *et al.* [5], there is a direct correlation between the bandgap of the host material and the optical efficiency of the RE^{3+} emission in a way that the luminescence thermal quenching decreases with increasing bandgap energy, making wide bandgap materials appropriate for the RE^{3+} optical activation [6,7]. In this sense, $Al_xGa_{1-x}N$ ternary alloys offer the possibility to tune the bandgap from 3.4 eV (GaN) to 6.2 eV (AlN), which is expected to provide favourable matrixes for RE incorporation and optical activation [8,9].

The semiconductor host and the ion lattice location inside the matrix play an important role as energy transfer sensitizer and to promote the RE^{3+} 4*f*→4*f* transitions probability, which are forbidden by Laporte's rule. Particularly, the local symmetry in which the ion is placed dictates the features of the ion-related emission, *e.g.* spectral shape and luminescence intensity. Thus, an appropriate choice of the semiconductor host and lattice location engineering can be used as a way to maximise the RE emission intensity [10]. In the case of GaN/AlN and related alloys, the RE ions tend to be located on cation (Ga and Al) sites where the lack of inversion symmetry gives rise to ligand fields promoting the states admixture, increasing the probability of the 4*f*→4*f* intraionic transitions, which results in the optical activation of the ions [9,11–14]. This substitutional incorporation, coupled with the strong bonds of the $Al_xGa_{1-x}N$ lattice, allows high doping levels (up to ~ 3-5 at%) without compromising the optical activation of the RE dopants [8,11]. In the review on RE incorporation in GaN by O'Donnell and Hourahine [10], the authors state that site location of the ions in the lattice seems to be independent of the doping method. Moreover, they showed that although the cation substitutional site (or slightly displaced) is the more frequent lattice site for RE incorporation, site multiplicity is very common in such samples. In fact, previous works in thulium (Tm) and terbium (Tb)-implanted $Al_xGa_{1-x}N$ samples [15–17] demonstrated that these ions have a tendency to occupy three preferential sites in the $Al_xGa_{1-x}N$ lattice: the cations' substitutional site, a site displaced by 0.2 - 0.3 Å along the c-axis

from the previous one and a random fraction. For the mentioned cases, the fraction of ions in the Al/Ga substitutional sites was found to be considerably higher (f_s > 63 %) than the remaining ones [15–18]. In fact, analysis of the spectroscopic features of the ion-related emission (taking into account the multiplet splitting due to the local crystalline environment) suggests that the strongest luminescence contribution is given by the substitutional ions. Thus, increasing the fraction of ions in such sites is expected to lead to an enhancement of the luminescence intensity (assuming negligible ion-ion interaction), which is beneficial when solid-state devices are envisaged. Nevertheless, it is important to take into account that the wide bandgap semiconductors typically used as matrixes for the ion incorporation frequently reveal broad emission bands in the ultraviolet and visible spectral regions due to native defects in the host material [19–22] which can impact the ions' emission intensity. Therefore, the study of such defects and their possible interaction with the dopant species should also be considered.

To accomplish the RE incorporation into the nitride matrixes, either *in-situ* or *ex-situ* methods have been employed. The former have the advantage of avoiding the damage of the crystal lattice induced by the *ex-situ* procedures and high crystal quality layers with a wide range of doping concentrations have been produced [10]. However, an adequate control of the RE concentration and uniformity over many orders of magnitude could be challenging [11]. On the other hand, *ex-situ* methods, as specifically ion implantation, offer many advantages since a control of the doping concentration can be achieved regardless of the growth conditions of the samples, even allowing for selective-area doping [11,23]. A crucial factor when ion implantation is chosen as the doping method is the damage formation during the process, which can create a number of non-radiative recombination paths that may affect the ion luminescence outcome [24,25]. Even though post-implantation thermal annealing is frequently employed both for optical activation and lattice recovery, partial damage frequently prevails [16,26,27]. To overcome this issue, it is essential to undertake procedures that may minimize the damage introduction during implantation. One example is to increase the substrate temperature above room temperature (RT) during the ion implantation process, which is expected to lead to a higher mobility of point defects, as vacancies or interstitials, favouring their recombination [16,27]. With this purpose in mind, $Al_xGa_{1-x}N$ ($0 \leq x \leq 1$) layers were implanted with Tb ions from RT to 550 ℃ [16]. The structural analysis of these samples revealed a complex behaviour where the defect concentration first increases when the implantation temperature is raised from RT to 100 ºC and then decreases again for higher temperatures. This trend is even preserved after annealing at 1200 ºC. Furthermore, the ion substitutional

fraction was seen to be higher for the highest implantation temperature for all the alloy compositions. The latter is expected to lead to improved luminescence, provided that a suitable control of the formation of possible non-radiative defects is achieved. As such, an adequate understanding of the influence of the formed defects in the excitation/deexcitation mechanisms and non-radiative processes of the RE ions in such processed nitride hosts is also crucial to evaluate their potential for optoelectronic applications. Therefore, the present work aims to shed light on the effect of the implantation temperature on the luminescence features of the ion-related luminescence, and correlate the results with the structural properties previously studied in reference [16]. Additionally, the impact of high-temperature implantation on the formation/enhancement of other optically active defects and their possible interaction with the emission of the implanted RE ions are studied. For this purpose, $Al_xGa_{1-x}N$ alloy layers (with x~0.2) were implanted with Tb ions at different substrate temperatures (RT to 550 ℃), and the effect of the implantation temperature on the behaviour of the host defects and intraionic Tb^{3+}-related emissions was investigated by means of photoluminescence (PL) and RT PL excitation (PLE) and time-resolved (TRPL). All the implanted and annealed samples exhibit the $^5D_4$-^7F_J intra-4*f*^{8} Tb^{3+} luminescence lines even at RT and the intensity of the ion's transitions was found to increase with increasing implantation temperature. Moreover, a correlation between the de-excitation processes involving the host defects and the observed thermal population of the Tb^{3+} emitting levels is discussed.

2. Experimental details

$Al_xGa_{1-x}N$ (x=0.20) layers (thickness ~ 565 nm), grown on (0001) sapphire substrates by metal organic chemical vapour deposition (MOCVD), were commercially acquired from NOVAGAN. The samples were implanted with Tb ions at 150 keV and a fluence of 7×10^{14} Tb cm^{-2}, with the beam aligned with the c-axis (channelled implantation) and implantation temperatures ranging from RT to 550 ℃, as reported elsewhere [16]. Post-implantation rapid thermal annealing (RTA) at 1200 ºC in flowing N_2 during 120 s was conducted to recover the lattice and to promote the optical activation of the ions. Note that, although the annealing temperature is much higher than the implantation temperature, previous structural characterisation revealed distinct defect structures in the samples even after annealing.

Steady-state PL was carried out using 325 nm (~3.81 eV) light from a cw He–Cd laser with an excitation power density less than 0.6 W cm^{-2}. The samples were mounted in a

cold finger of a closed-cycle helium cryostat and the sample's temperature was controlled in the range between 14 K and RT. The luminescence was measured using a dispersive system SPEX 1704 monochromator (1 m of focal length, equipped with a 1200 grooves mm^{-1} diffraction grating blazed at 435 nm and with a dispersion of 0.8 nm mm^{-1}) fitted with a cooled Hamamatsu R928 photomultiplier tube. Excitation density-dependent PL studies were conducted in the same equipment and with the same excitation source, using neutral density filters.

RT PLE experiments were performed in a Fluorolog-3 Horiba Scientific modular system, equipped with a double additive grating Gemini 180 scanning monochromator (1200 grooves mm^{-1} diffraction grating blazed at 330 nm and with a dispersion of 2.1 nm mm^{-1}) for excitation, while for the emission an iHR550 spectrometer (1200 grooves mm^{-1} diffraction grating blazed at 500 nm, with a dispersion of 2.35 nm mm^{-1}) coupled to a R928P photomultiplier was used in the front face acquisition mode. A 450 W Xe arc lamp was used as excitation source. These measurements were conducted setting the emission monochromator either at the Tb^{3+} emission lines or the maximum of the broad visible band and the excitation wavelength was scanned to higher energies. . RT time-resolved (TRPL) spectra were acquired with the same Fluorolog-3 system using a pulsed Xe lamp (operating at up to 25 Hz) coupled to the same monochromators and with the excitation fixed at 325 nm. The full-width at half-maximum of each lamp pulse is 3 μs, so that lamp interference during acquisition of decay curves is minimized. The measurement conditions were set to a sample window (duration of signal acquisition) of 10 ms, with 60 ms of time per flash (reciprocal of the repetition rate of the lamp pulses) and a flash count (number of lamp pulses contributing to each data point) of 200. Several time delays after flash were employed from 0.05 to 10 ms.

3. Results and discussion

3.1. Low temperature steady-state PL

Figure 1a shows the 14 K PL spectra obtained by exciting the samples with 325 nm (~3.81 eV) photons, which corresponds to above bandgap excitation for the present $Al_{0.20}Ga_{0.8}N$ layers. The spectra reveal that the optical activation of the Tb^{3+} ions was successfully achieved for all the implanted and annealed samples. In addition to the intra-shell luminescence, the whole set of samples exhibits host defect-related broad emission bands in the ultraviolet (UV)/blue and yellow spectral regions (the latter peaked at ~540 nm) overlapped with the ion emission. It is worth to mention that a slight shift in the peak position of the yellow band is observed between the as-grown

and the implanted and annealed samples (from ~525 nm to ~540 nm). As will be discussed below, several hypotheses have been proposed for the origin of this defect-related emission and distinct defects are known to give rise to luminescence features with similar spectral shape and even analogous peak position. Even so, the shift observed for the band maxima is in line with previous results obtained from our group in GaN nanostructures, evidencing that both implantation and thermal annealing may induce/promote defects that give rise to the yellow luminescence (YL) [28]. Thus, a similar effect may have occurred in the present samples, resulting in the formation of additional optically active defects emitting in the yellow spectral region. Concerning the UV/blue bands, different features were found for the used implantation temperatures, in a similar way to what was previously identified in other $Al_xGa_{1-x}N$ samples [18,29]. In the case of AlN samples, wide unstructured emission bands are commonly attributed to oxygen-related defects , with maxima in the near-UV (~400 nm; ~3.1 eV), and native defects peaked at the blue spectral region (~480 nm; ~2.58 eV) [30–32]. Assuming an analogous chemical nature of defects for the present alloy, the differences observed for the employed implantation temperatures may be attributed to distinct defect concentration/diffusion depending on the applied substrate temperature during implantation. Note that luminescence features in this spectral region were already present in the as-grown sample, even with a higher intensity than the broad yellow band.

Regarding the intraionic $^5D_4 \rightarrow {}^7F_J$ (J=6, 5, 4 and 3) emission lines, it is clearly seen that their relative intensity is enhanced as the implantation temperature increases, when compared to the broad defect band emission. In the previous study concerning the defect formation as a function of the implantation temperature, reported in reference [16], it was shown that the damage concentration in this set of samples increases when the implantation temperature is raised from RT to ~100-140 ºC, and then drops rapidly for implantation at 200 ºC, followed by a new increasing when the temperature is raised up to 550 ºC. Besides, Rutherford Backscattering Spectrometry (RBS) data [16] revealed that a higher substitutional fraction was obtained for the highest implantation temperature. Thus, the observed enhancement in the intensity of the ion emission lines is most likely due to the higher concentration of optically activated Tb^{3+} ions in the cation sites for this implantation temperature. The highest relative intensity was observed for the $^5D_4 \rightarrow {}^7F_6$ transition, at ~491 nm, followed by the $^5D_4 \rightarrow {}^7F_5$ (~549 nm) recombination. Minor intensity lines attributed to $^5D_4 \rightarrow {}^7F_4$ (584 nm) and $^5D_4 \rightarrow {}^7F_3$ (~626 nm) were also detected (see a high-resolution spectrum for the sample implanted at 550 ºC in Figure 1 b). As mentioned in the introduction, previous studies in

Tb-implanted $Al_xGa_{1-x}N$ samples [16,17] revealed that the ions tend to preferentially occupy substitutional cation sites (substitutional fraction ~ 63 % and 70 %, for RT and 550 ºC implantation temperatures, respectively), with only small fractions slightly displaced from the regular site or randomly distributed in the matrix. For Tb^{3+} ions in such a local environment (C_{3v} coordination symmetry), the degeneracy of the ion multiplets is broken by the crystalline field of the host and a state with J=6, 5 or 4 is expected to split in a total of nine, seven or six energy levels, respectively [29,33]. However, in the present case, the number of observed lines is lower than the expected for a full degeneracy lifting (see Figure 1b).This is likely due to the sensitivity of these transitions to the alloy disorder, which broadens the emission lines and prevents close lines to be resolved. It is well known that disorder effects tend to appear in the ternary nitride alloys. In particular, the alloy broadening values of the intraionic transitions, compared to the corresponding ones for the binary systems (see reference [29]), is also an evidence of disorder effects. Furthermore, it is important to take into account that the overlapping with the broad yellow band may obscure some of the expected ion-related emission lines.

3.2. Excitation density-dependent and time-resolved PL

Excitation density-dependent PL studies were conducted to gain better insight regarding the nature of the yellow band recombination in the present $Al_{0.2}Ga_{0.8}N$ alloys. For this purpose, two samples were selected from the whole set: implanted at 140 ºC and 300 ºC. These samples were chosen since they correspond to the highest and lowest damage concentration, respectively (according to the prior RBS results [16]), allowing to infer if there is any effect of the defect concentration on the behaviour of this optical centre. The results show that a similar behaviour was found for the YL in the two samples, suggesting that the nature of the emission is independent on the damage concentration. In both cases, no shift of the yellow band was observed with the used excitation densities, meaning that the YL behaves differently than what would be expected for a typical donor-acceptor pair (DAP) recombination. The YL was well fitted using a single Gaussian function (not shown), allowing to extract important information, as for instance PL intensity, peak position and full width at half maximum. As a function of the excitation density, the PL intensity of the YL (Figure 2) can be well fitted to a power law, $I \propto P^m$, where I is the luminescence intensity, P is the excitation power and m is a parameter that represents the slope in a log-log representation of I and P, as reported by T. Schmidt *et al*. [34]. The analysis reveals a slope of 0.91 ± 0.01 and 0.96 ± 0.02 for the samples implanted at 140 ºC and 300 ºC, respectively. According to the

same authors [34], m<1 proposes that the nature of the radiative transitions involves either a DAP or a free-to-bound carrier recombination. However, the presence of DAP was not corroborated by the change in the PL peak position. To obtain further information about the possible nature of this emission, TRPL measurements were conducted at RT in the same samples (140 ºC and 300 ºC) and the results are depicted in Figure 3. Time delays between 0.05 ms and 10 ms were employed and, as can be seen in Figure 3, the broad band does not seem to shift with increasing time delay in either case. Typically, DAP recombination evidences a well-defined behaviour both under excitation density and under time-dependent studies. When low excitation densities are applied, only a fraction of the pairs are excited, leading to the recombination of only the distant pairs. By increasing the excitation density, more pairs become excited, resulting in an additional contribution from the closer pairs to the recombination spectra. This contribution gives rise to a shift of the emission spectra to higher energy with the increase of the excitation density, which is a characteristic feature of the DAP recombination. Moreover, this type of recombination also shows time dependence after excitation by a short pulse. When all the donors and acceptors are excited, the transition probability of recombination is faster for closer pairs, as a higher overlap degree of the carriers' wavefunctions occurs. On the other hand, distant pairs show a low overlap of the carriers' wavefunctions, resulting in lower probability transitions and longer lifetimes. Therefore, the recombination spectra are expected to show a shift towards lower energies with increasing time delays, resulting in a redshift of the emission and a non-exponential time decay [35,36]. The fact that, in the present case, no shift in the peak position of the band was observed neither for excitation density nor time dependences suggests that a free-to-bound transition should be considered rather than a DAP recombination. In fact, nowadays it is well established that undoped and doped GaN layers typically exhibit a broad YL described by DAP (involving a shallow donor) or e-A transitions to the same defect [21,37–42]. Although, in the case of $Al_xGa_{1-x}N$ alloys this defect band has not been much explored, it is fair to assume that for an alloy with such a low AlN molar fraction (x~0.2), the origin of the band should be related to the one reported for GaN. Currently, it is commonly believed that the YL in GaN is associated with the presence of native defects, namely V_{Ga} and their $V_{Ga}O_N$ complexes in the 2-/- charge states [21,37–43]. It is well known that in the same spectral region, different types of defects can be found, giving rise to similar broad emissions. For instance, Reshchikov and co-workers proposed that, in the case of *n*-type GaN grown by hydride vapour phase epitaxy (HVPE), the YL band with a maximum at 2.1 eV is caused by a recombination of free electrons with holes at the −/0 level of C_N at low excitation intensities, which is replaced by the green luminescence

(GL) band at high excitation intensity, in a similar way with what was reported earlier by the same author considering the $V_{Ga}O_N$ complex [41]. Latter, the same authors [44] claimed that no correlation was found between the YL and GL bands. The authors analysed a large number of GaN samples and could only observe the YL associated with transitions via the −/0 level of the C_N defect, no band associated to the 0/+ level was identified. Nevertheless, they present strong evidences of the correlation between the YL peaked at 2.20 eV (at low temperature) and a carbon-related defect, which has a thermodynamic charge transition level at 0.916 eV above the valence band maximum [44]. Also Lyons *et al.* [45,46] reported theoretical studies where they found that the broad emission at 2.14 eV is indeed related to C_N. Moreover, carbon impurities forming complexes with oxygen (C_NO_N) may also account for a YL band at 2.2 eV [47,48]. Indeed, carbon contamination cannot be disregarded in the case of samples produced by MOCVD, as the present ones, due to the decomposition of the precursors involved in the growth process [16,49,50].

Even though the TRPL measurements were conducted in order to assess the nature of the defects responsible for the YL, information regarding the lifetime of both the broad visible emission and the $^5D_4$-^7F_J intra-4f^8 transitions can also be inferred from the obtained results. However, due to the low signal-to-noise ratio recorded for such excitation, the deconvolution of the present optical centres is not possible, and thus, a proper value for decay time of the different emissions (as was performed in Ref. [29]) cannot be extracted. Nevertheless, the experimental data allow to conclude that, in both analysed samples, the YL intensity quenches faster than the ion emission. The broad band is seen to nearly disappear after a time delay of ~0.75 ms, while the ion-related emission lines prevail even after 5 ms. For the later, an intensity decrease of about one order of magnitude after ~ 2 ms was observed, indicating a lifetime in the range of a few ms. Such lifetime range is slightly higher than the one recorded in our previous studies in $Al_xGa_{1-x}N$:Tb (hundreds of µs) [29]. In that case, however, the intensity of the $^5D_4$-^7F_J intra-4f^8 transitions (at RT) for the alloy with a composition similar to the one presented here was not enough to access the lifetime of these transitions. Nonetheless, it was observed that the lifetime increased with increasing Al molar fraction, thus, a lifetime shorter than ~200 µs was expected, which is in line with the values also reported by Wakahara *et al.* [7,51]. Though, there are other reports on Tb-implanted nitrides, as for instance by Lozykowski *et al.* [52] in GaN layers, where longer decay times, in the range of ms, were measured. These differences can be related to the presence of different types/density of defects depending on the analysed samples, since the crystalline and optical quality of these alloys are known to be highly

dependent on the growth procedure. In fact, comparing the set of samples evaluated in the present paper with the one previously reported in reference [29], we observed that, for instance, the YL is not peaked at the same position, even comparing similar Al molar fraction. This fact evidences that different defects are likely to be present in the samples, giving rise to different interactions with RE ions. Indeed, in the present case, thermal population of the ion related emission was observed, as will be highlighted in the following section. Such phenomenon may even give rise to a PL decay behaviour different from a single-exponential one found in our previous samples. In fact, multiexponential behaviours have been reported in the literature for Tb-doped $Al_xGa_{1-x}N$ [7,53]. Deviations from a single exponential law are typically an indication of the presence of nonradiative phenomena, such as multiphonon relaxation and energy transfer processes [54]. Unfortunately, as stated above, our TRPL data do not allow a proper determination of the decay behaviour, hampering further conclusions.

3.3. Temperature-dependent PL

With the purpose of exploring in more detail the recombination processes, temperature-dependent PL was carried out between 14K and RT. As can be seen in Figure 4, a strong thermal quenching of the luminescence intensity is observed for the visible broad emission and, as the temperature rises, the spectra become dominated by the intraionic Tb^{3+} emission for all samples implanted with temperatures higher than RT. In the case of the one implanted at RT, the intensity of the intraionic emission remains considerably weak when compared with the yellow band, even at RT.

As mentioned in the case of the excitation density-dependent PL studies, the yellow band can be well fitted by a single Gaussian function over all the range of temperatures. It was observed that, for all samples, the broad band shifted its energy peak position as a function of the temperature, evidencing an atypical red-blueshift behaviour, as demonstrated in Figure 5. For temperatures up to 90 – 110 K, the energy peak position decreases, while for higher temperatures this value increases with increasing temperature. This kind of behaviour is frequently found in semiconductor alloys, including $Al_xGa_{1-x}N$ and $In_xGa_{1-x}N$ [55–57], and is often attributed to inhomogeneous potential fluctuations caused by alloy disorder [58]. Statistical fluctuations in the composition of a random alloy generally lead to potential fluctuations capable of spatially localising carriers [55]. As reported by Chung *et al*. [59], as the temperature slightly increases, weakly localised carriers are thermally excited and would either recombine non-radiatively or redistribute to other strongly localised states. Thus, the PL energy peak position decreases with increasing temperature. After the effect of redistribution is saturated, the thermal energy can excite carriers to higher

localised states, and hence, the PL peak energy increases [59]. According to Bell *et al.* [55], at that stage, the carriers freeze-out and do not have enough thermal energy to overcome the potential barrier, becoming trapped in local minima with no further relaxation. In such case, the energy peak position saturates and can even increase with decreasing temperature, leading to a *s*-shape dependence [55].

Even though this phenomenon has been widely reported for the near band edge (NBE) emission in $Al_xGa_{1-x}N$ alloys [55,59–61], less attention has been paid to the visible defect-related emission. Taking into account an alloy with AlN molar fraction similar to the one reported here, the *s*-shape behaviour described for the NBE emission typically shows an increase in the energy peak position for temperatures up to 50 – 80 K, with a further decrease for higher temperatures [55,59,60]. However, in the case of the yellow emission, the increase in the peak position is observed for temperatures higher than 110 K up to RT, which constitutes a much higher temperature for the freeze-out of the carries than the one reported for the NBE. Since the temperature at which exciton freeze-out occurs can give an indication of the barrier height [55], and taking into account the energy shift observed for the peak position, it is fair to assume that, in the present case, the potential barrier is in the order of ~100 meV, which is much higher than the one typically found for the NBE recombination.

It is interesting to note that, for the case of the sample implanted at RT, the peak position of the broad band was found at lower energy values when compared to the remaining samples (except when measured at 14 K, where the peak position is similar in all samples, ~2.3 eV/~540 nm). Even though the same trend in the red-blueshift behaviour occurs, the redshift at lower temperatures is more pronounced in this case, achieving a minimum value of ~2.23 eV at 90 K. The subsequent temperature increase leads to a blueshift up to ~2.35 eV at RT, while for the samples implanted at higher temperatures the peak position of the yellow band at RT is ~2.41-2.42 eV. This difference in the peak position may be explained by different potential fluctuations in this sample. The implantation process is known to cause intermixing and randomise the composition of the implanted samples [62], which may lead to changes in the local potential fluctuations depending on the implantation conditions. At the same time, implantation damage processes in $Al_xGa_{1-x}N$ ($0 \leq x \leq 1$) alloys present strong dynamic annealing effects, which means that point defects are mobile and can recombine more easily [24,25]. This mobility is promoted by increasing the implantation temperature [16,24,25] and thus, keeping the substrate at temperatures higher than RT may partially mitigate the formation of additional defects that may contribute to changes in potential fluctuations. Moreover, the higher fraction of Tb^{3+} ions displaced along the c-

axis found for the RT sample (27% *vs* 17% obtained for the sample implanted at 550 ºC) [16] may be related to the difference in the potential fluctuations. This can lead to the distinct behaviour in the peak position of the YL, namely due to an increase in the interaction of the Tb^{3+} ions with the defects.

Regarding the intensity of the broad YL band, the values were seen to decrease with increasing temperature, for all samples. Under the assumption that the non-radiative recombination processes can be treated classically by a Mott law, the temperature dependence of the integrated intensity is well described by

$$\frac{I(T)}{I_0} = \frac{1}{1 + C_1 \exp(-E_{a1}/k_B T) + C_2 \exp(-E_{a2}/k_B T)} \quad (1)$$

considering two activation energies for the thermal quenching. In this expression I_0 stands for the intensity at the lowest measured temperature (14 K), $C_{1,2}$ correspond to the pre-exponential factors which account for the energy level degeneracy, k_B is the Boltzmann constant, T is the absolute temperature and $E_{a1,2}$ stand for the activation energies of the non-radiative processes. The best fit to the proposed model (full line in Figure 6) leads to the activation energies depicted both in Figure 6 and in Table 1. From these results it is possible to conclude that non-radiative processes are present for all the implanted and annealed samples, even at low temperatures, as can be seen by the significant PL intensity decrease observed in that region. A similar behaviour was also found for other RE doped $Al_xGa_{1-x}N$ alloys [18].

Enlarged and high-resolution spectra of the intra-shell $^5D_4 \rightarrow {}^7F_6$ transition obtained between 14 K and RT are depicted in Figure 7. The spectra represented in Figure 7 correspond to the ion-related PL signal after spectral deconvolution using the fitted YL as baseline. For samples implanted at temperatures higher than RT, the intensity of this transition was seen to decrease with increasing temperature, up to ~100 K, followed by an increase for higher temperatures up to ~200 – 230 K, with a subsequent decrease up to RT. This behaviour can be better observed in Figure 8 where the normalised integrated intensity *vs* temperature is displayed (the integrated area of the $^5D_4 \rightarrow {}^7F_6$ transition was determined by numerical integration in the correspondent spectral range). The lower intensity observed for the RT implantation is likely related with the lower Tb substitutional fraction on cation sites and higher ion displacement found in this case. Tb ions on the displaced sites (~0.2 Å along the c-axis from the cation site) may indicate the formation of defect complexes [16], which may result in a higher quenching of the ion related emission. Thus, in the case of the intraionic $^5D_4 \rightarrow {}^7F_6$ transition observed for samples implanted at temperatures higher than RT,

the variation of PL intensity with the temperature, *I(T)*, can be described by a multi-level model [63], which, in this case, can be expressed as

$$\frac{I(T)}{I_0} = \frac{1 + D_1 \exp(-E_p/k_B T)}{1 + D_2 \exp(-E_{d1}/k_B T) + D_3 \exp(-E_{d2}/k_B T)}. \qquad (2)$$

This model takes into account the increase and decrease of the luminescence intensity, where $D_{1,2,3}$ are the corresponding weight factors, E_p describes the activation energy for a process that increases the PL intensity with increasing temperature while $E_{d1,2}$ correspond to the activation energies for non-radiative channels [64,65]. The fitted activation energies found for the different samples are summarised in Table 1. The existence of non-radiative recombination channels even at such low temperatures can be associated with carrier trapping/detrapping in defect centres. In fact, the material's quality assumes a relevant role, not only in the line broadening observed above, which increases with increasing disorder in the alloys, but also by the introduction of non-radiative channels. These non-radiative channels compete with the radiative luminescence, inhibiting the determination and attainment of high internal quantum efficiencies, which are of utmost relevance to the fabrication of the optoelectronic devices.

The experimental data were fitted by equation (2) and the results are plotted in Figure 8. In the present case, it was found that for samples implanted with temperatures higher than RT, the activation energy for the population is in good agreement with the one obtained for the de-excitation mechanism of the host defect centre (see Figures 6 and 8), suggesting a correlation between the de-excitation processes of the broad visible band and the increasing Tb^{3+} emission intensity. As mentioned before, in the case of the sample implanted at RT, the intensity of the $^5D_4 \rightarrow {}^7F_6$ transition was found to be very weak when compared to the intensity of the broad band (Figure 7a), hampering a proper determination of its integrated intensity and thus an adequate fit of the resulting data (Figure 8a). It is also important to mention that no clear correlation between the defect concentration (which decreases in the following order: 140 ºC > 550 ºC > RT > 300 ºC [16]) or the implantation temperature and the activation energies obtained for either the YL or the ion-related emission could be established. Only in the case of the ion's depopulation energy a tendency could be proposed, with the energy value increasing with increasing defect concentration, likely related with the presence of a higher concentration of non-radiative defects in the alloy.

The present results regarding the activation energies contrast with the ones previously obtained by our group in $Al_xGa_{1-x}N$ ($0 \leq x \leq 1$) implanted with similar fluence

(5×10^{14} Tb.cm^{-2}) of Tb at RT [29], where a single activation energy was found to describe the thermally activated non-radiative paths for the ion-related emission in all the alloy range. However, it is worth to mention that the layers were grown by different techniques (HVPE *vs* MOCVD) and thus different types of defects are expected to be present, as well as different potential fluctuation due to distinct alloy disorder, leading to significant differences in the recombination processes present in both sets of samples. As previously stated, even though broad visible bands in the yellow spectral region were detected in both cases, slight displacement of the band peak position at 14 K is observed when one compares the samples here reported with the one of reference [29] with similar AlN molar fraction (x=0.19). In the first case, the band is peaked at ~540 nm, while for the latter a maximum at ~528 nm was found, indeed pointing out to the distinct nature of the defects involved and/or different quality of the samples. Thus, it is fair to assume that different defect centres will have distinct interactions with the implanted ions, leading to different thermally activated de-excitation processes.

Previous work by Wakahara [7,66] in Tb-doped $Al_xGa_{1-x}N$ ($0\leq x\leq 1$) samples grown by organometallic vapour phase epitaxy also reported an increase in the PL intensity in the temperature range of 100–200 K for samples comprising a high Al content ($x>0.7$). The author attributed this behaviour to the presence of trap levels, which may act as an energy reservoir, trapping photoexcited carriers at low temperatures that can be thermally de-excited at high temperatures and captured by the energy transfer centre for Tb^{3+} [7,51,66]. According to the model proposed by these authors, the behaviour observed for the temperature dependence of Tb^{3+} in AlGaN can be explained by the same energy transfer model proposed for a luminescence mechanism in other RE^{3+}-doped nitrides [67–70], accessible via multi-phonon assisted processes. This point will be further discussed in the next section concerning the RT PLE results. In the here reported case, this role is likely to be played by the defects that originate the yellow luminescence, as suggested by the similar values obtained for the activation energies of the de-excitation mechanism of the YL and the ion population mechanism.

Table 1 – Activation energies obtained from the fits in Figure 6 and 8 using Eq. (1) and Eq. (2), respectively. *Considering the intensity at 30 K as I_0 (I_{LT}). The text in bold highlights the similarity between the values obtained the population of the ion-related emission and the de-excitation of the host defect centre for each implantation temperature.

Samples	**Activation energy**		
	Visible band	$^5D_4 \rightarrow {}^7F_6$ transition	
		Population	Depopulation
Imp. RT	E_{a1}= 7.7 ± 3.7 meV E_{a2}= 53.4 ± 6.1 meV	-	-
Imp. 140 ºC	E_{a1}= 1.8 ± 4.4 meV **E_{a2}= 42.2 ± 5.2 meV**	**E_p= 38.3 ± 3.8 meV**	E_{d1}= 2.3 ± 0.3 meV E_{d2}= 244.8 ± 16.7 meV
Imp. 300 ºC*	E_{a1}= 1.5 ± 0.4 meV **E_{a2}= 44.1 ± 3.7 meV**	**E_p= 43.3 ± 8.1 meV**	E_{d1}= 4.5± 0.9 meV E_{d2}= 135.5 ± 5.9 meV
Imp. 550 ºC	E_{a1}= 3.9 ± 3.9 meV **E_{a2}= 33.5 ± 4.57 meV**	**E_p= 34.0 ± 4.8 meV**	E_{d1}= 1.5 ± 0.4 meV E_{d2}= 230.0 ± 18.8 meV

3.4. RT PLE studies

In order to acquire more in-depth information about the preferential excitation pathways of the Tb^{3+} ions' levels in the present set of samples, RT PLE spectra were monitored at the energy position of the intra-shell transitions, as well as at the maximum of the broad defect band, as shown in Figure 9a. It is important to bear in mind that, as an overlap of emitting centres occurs, the PLE measurements simultaneously assess the excitation population mechanisms of the host defect responsible for the broad band and the ion luminescence. As evidenced in Figure 9a, similar excitation spectral features were observed for all samples. A well-defined excitation band with a maximum at ~332 nm (~3.73 eV) can be identified when the excitation is monitored both at the ion-related emission (~554 nm/2.24 eV) and visible band (~510 nm/2.43 eV). This value matches well the expected bandgap for a ternary alloy with this Al molar fraction (assuming a bowing parameter b=1.3 [71]), suggesting that both the defect-related band and the $^5D_4$ Tb^{3+} emitting level are favourably excited through above bandgap excitation. This behaviour indicates an efficient energy transfer from the host to the Tb^{3+} excited levels, as we previously reported for these alloys [29]. Particularly, the ions' population is preferentially mediated through the exciton generation and their energy transferred to the ion. This assumption is also corroborated by the similar values obtained for the activation energies of the host defect de-excitation and the

population of the $^5D_4$ level, as discussed above. Namely, it is fair to assume that the thermal quenching of the broad band leads to an increase of free carriers in the host, resulting in a higher concentration of formed excitons, which will feed the ions luminescence. Additionally, a broadening of the band edge absorption is observed in the PLE spectra with increasing damage concentration (previously obtained by RBS measurements [16]). Such behaviour suggests an increase of defect-related states in the population pathways of both the broad yellow emission and ion-related transitions due to implantation damage.

Besides the bandgap, additional subgap excitation bands/shoulders were detected, namely at 368 nm (~3.36 eV) and 373 nm (~3.32 eV). In fact, when monitored at ~420 nm (~2.95 eV), corresponding to the UV/blue band, the PLE spectra are dominated by a broad excitation band centred around 373 nm, evidencing that this is the preferential pathway for the population of that defect, rather than bandgap excitation.

On the other hand, when monitored at 554 nm ($^5D_4 \rightarrow {}^7F_5$ transition), a shoulder at 368 nm (~3.36 eV) is detected, which is likely related to the excited levels of the Tb^{3+} ion since it only appears when the ion emission is monitored. This energy position is in line with what would be expected for the $^5D_4$ level in an alloy with such Al content (x~0.20), considering the atomic-like model previously described [29] and the one proposed by Dorenbos *et al*. [72,73]. This implies that population of the ions' excited states via direct excitation is likely to occur and different excitation processes for the ion-related emission may be present at the same time. However, since it is overlapped with the broad defect-related excitation band, excitation in this region favours the observation of the host defect luminescence, dominating over the Tb^{3+}-related transitions (see Figure 9b). Figure 9b shows RT PL spectra acquired for the sample implanted at 300 ºC using different excitation energies. For all the energies used, the host defect luminescence dominates over the Tb^{3+} transitions. Indeed, a strong contribution of the UV/blue emission band was identified for both above and below bandgap excitations, almost masking the ion emission, meaning that the defect population is favoured over the Tb^{3+} excited states, even when energies resonant with the excitation paths of the ion are used. Furthermore, when excited at the maximum of the broad excitation band (370 nm), the strong defect band completely dominates the PL spectrum, hindering the observation of the ion-related emission.

Assuming the presence of an energy transfer centre for the RE ion implies the contribution of indirect excitation paths for the population of the excited levels of the Tb

ions. In fact, different excitation mechanisms have been proposed for the RE ions incorporated into semiconductor matrixes, being divided into direct and indirect. In the first case, the excitation is resonant with the high energetic levels of the RE inner 4*f* shell, while the indirect mechanisms are non-resonant and occur by non-radiative energy or charge transfer from the host, usually called host sensitisation [12,68]. In our previous paper reporting the detailed spectroscopic study of Tb-doped HVPE grown $Al_xGa_{1-x}N$ ($0 \leq x \leq 1$) samples [29], excitation models were discussed based on the most well-accepted mechanisms presented in the literature. The discussion was focused essentially on two models, one extensively supported by Lozykowski and co-workers [67,68,70], where the REs are treated as isoelectronic impurities and the RE excitation is accomplished by energy transfer mechanisms, and another widely developed by Dorenbos [72–76], which predicts the 4*f*-level location regarding the conduction and valence bands of the semiconductor host. In the latter, the behaviour of the RE ions is explained by the change in the ions' valence charge instead of energy transfer [68]. In our previous work on the Tb-doped $Al_xGa_{1-x}N$ layers [29], a schematic energy diagram similar to the one proposed by Dorenbos [72] was constructed based on peak position of the PLE band maxima as a function of the alloy composition. This diagram allowed the energetically positioning of the Tb^{3+} multiplets and 5d states with respect to the conduction and valence band of the $Al_xGa_{1-x}N$ alloy. According to this diagram, it is expected that the $^5D_4$ Tb^{3+} emitting level (observed also in the present samples) is placed at an energy around ~3.35 eV (above the valence band) for an alloy with x~0.2. In fact, as mentioned above, our experimental results revealed a shoulder at ~3.36 eV when monitored at the $^5D_4 \rightarrow {}^7F_5$ transition, which may indicate resonant excitation to the ions' excited levels. Thus, direct excitation cannot be ruled out and both excitation mechanisms should be considered for the population of the ions' excited levels in the present set of samples.

4. Conclusions

$Al_{0.2}Ga_{0.8}N$ samples implanted with terbium ions at different temperatures and annealed at 1200 ºC were studied by luminescence techniques. All studied samples exhibit green light from the characteristic Tb^{3+}-related lines originated from the $^5D_4$ emitting level. When compared with the broad defect band, the intensity of the ion emission was seen to increase with increasing implantation temperature, with the sample implanted at 550 ºC revealing the highest intensity for the $^5D_4 \rightarrow {}^7F_J$ transitions. Excitation density and time-resolved measurements were carried out in order to gain some insights

regarding the nature of the defects responsible for the yellow emission in the here reported samples. The results indicate that this emission exhibits a behaviour different from the one that would be expected for a donor-acceptor pair transition, suggesting a different nature for the transition. It was observed that the energy peak position of the broad evidences an s-shape behaviour with increasing temperature. Even though such phenomenon is well-known for the ultraviolet emission in $Al_xGa_{1-x}N$ alloys and typically attributed to the presence of inhomogeneous potential fluctuation caused by alloy disorder, less attention has been paid to the yellow luminescence induced/enhanced by the implantation process, as reported in the present work. Additionally, the intensity of the yellow luminescence was found to decrease with temperature for all studied samples, with the thermal quenching of the luminescence well accounted by a classical model which considers two activation energies. The ion-related luminescence was found to be thermally populated with increasing temperature, being described by a multi-level model with one activation energy for the population and two activation energies for the non-radiative channels. The population energy matches well one of the activation energies obtained for the de-excitation of the yellow band, suggesting that a correlation between the de-excitation processes of the host defect and the population of the ion emitting levels may be present, as also corroborated by the photoluminescence excitation results.

Acknowledgements

The authors acknowledge financial support from FEDER funds through the COMPETE 2020 Programme and National Funds through FCT - Portuguese Foundation for Science and Technology under the projects UID/CTM/50025/2013, POCI-01-0145-FEDER-028011 & LISBOA-01-0145-FEDER-029666.

References

[1] L. Bodiou, A. Braud, J.-L. Doualan, R. Moncorgé, J.H. Park, C. Munasinghe, A.J. Steckl, K. Lorenz, E. Alves, B. Daudin, Optically active centers in Eu implanted, Eu in situ doped GaN, and Eu doped GaN quantum dots, J. Appl. Phys. 105 (2009) 043104. doi:10.1063/1.3078783.

[2] Z. Fleischman, P.S. Tafon, V. Dierolf, C. Munasinghe, A.J. Steckl, Identification

of defect-trap-related europium sites in gallium nitride, Phys. Status Solidi C. 4 (2007) 834–837. doi:10.1002/pssc.200673822.

[3] A.J. Kenyon, Recent developments in rare-earth doped materials for optoelectronics, Prog. Quantum Electron. 26 (2002) 225–284. doi:10.1016/S0079-6727(02)00014-9.

[4] J. Rodrigues, S.M.C. Miranda, N.F. Santos, A.J. Neves, E. Alves, K. Lorenz, T. Monteiro, Rare earth co-doping nitride layers for visible light, Mater. Chem. Phys. 134 (2012) 716–720. doi:10.1016/j.matchemphys.2012.03.056.

[5] P. Favennec, H. L'haridon, Luminescence of erbium implanted in various semiconductors: IV, III-V and II-VI materials, Electron. Lett. Lett. 25 (1989) 718–719. doi:10.1049/el:19890486.

[6] M.R. Soares, J. Rodrigues, N.F. Santos, C. Nico, R.G. Carvalho, A.J.S. Fernandes, M.P. Graça, L. Rino, M.J. Soares, A.J. Neves, F.M. Costa, T. Monteiro, Prospects on laser processed wide band gap oxides optical materials, in: F.H. Teherani, D.C. Look, D.J. Rogers (Eds.), SPIE OPTO, International Society for Optics and Photonics, 2013: p. 862607. doi:10.1117/12.2016508.

[7] A. Wakahara, Impact of AlGaN on luminescence capability of rare-earth ions in AlGaN, Opt. Mater. (Amst). 28 (2006) 731–737. doi:10.1016/j.optmat.2005.09.011.

[8] N. Nepal, S.M. Bedair, N.A. El-Masry, D.S. Lee, A.J. Steckl, J.M. Zavada, Correlation between compositional fluctuation and magnetic properties of Tm-doped AlGaN alloys, Appl. Phys. Lett. 91 (2007) 222503. doi:10.1063/1.2817741.

[9] K. Wang, K.P. O'Donnell, B. Hourahine, R.W. Martin, I.M. Watson, K. Lorenz, E. Alves, Luminescence of Eu ions in $Al_xGa_{1-x}N$ across the entire alloy composition range, Phys. Rev. B. 80 (2009) 125206. doi:10.1103/PhysRevB.80.125206.

[10] K.P. O'Donnell, B. Hourahine, Rare Earth Doped III-Nitrides for Optoelectronics, Eur. Phys. J. - Appl. Phys. 36 (2006) 91–103. doi:10.1051/epjap:2006122.

[11] A.J. Steckl, J.C. Heikenfeld, M.J. Garter, C.C. Baker, R. Jones, Rare-earth-doped GaN: growth, properties, and fabrication of electroluminescent devices, IEEE J. Sel. Top. Quantum Electron. 8 (2002) 749–766. doi:10.1109/JSTQE.2002.801690.

[12] K.P. O'Donnell, Rare-Earth Doped III-Nitrides for Optoelectronic and Spintronic Applications, Springer, 2009.

[13] T. Monteiro, C. Boemare, M.J. Soares, R.A. Sá Ferreira, L.D. Carlos, K. Lorenz, R. Vianden, E. Alves, Photoluminescence and lattice location of Eu and Pr implanted GaN samples, Phys. B Condens. Matter. 308–310 (2001) 22–25. doi:16/S0921-4526(01)00656-1.

[14] K. Lorenz, E. Alves, F. Gloux, P. Ruterana, M. Peres, A.J. Neves, T. Monteiro, Optical doping and damage formation in AlN by Eu implantation, J. Appl. Phys. 107 (2010) 023525. doi:10.1063/1.3291100.

[15] M. Fialho, K. Lorenz, S. Magalhães, J. Rodrigues, N.F. Santos, T. Monteiro, E. Alves, Lattice site location and luminescence studies of $Al_xGa_{1-x}N$ alloys doped with thulium ions, Nucl. Instruments Methods Phys. Res. Sect. B Beam Interact. with Mater. Atoms. 307 (2013) 495–498. doi:10.1016/j.nimb.2013.01.010.

[16] M. Fialho, S. Magalhães, J. Rodrigues, M.P. Chauvat, P. Ruterana, T. Monteiro, K. Lorenz, E. Alves, Defect formation and optical activation of Tb implanted $Al_xGa_{1-x}N$ films using channeled implantation at different temperatures, Surf. Coatings Technol. 355 (2018) 29–39. doi:10.1016/j.surfcoat.2018.02.008.

[17] M. Fialho, J. Rodrigues, S. Magalhães, M.R. Correia, T. Monteiro, K. Lorenz, E. Alves, Effect of AlN content on the lattice site location of terbium ions in $Al_xGa_{1-x}N$ compounds, Semicond. Sci. Technol. 31 (2016) 035026. doi:10.1088/0268-1242/31/3/035026.

[18] J. Rodrigues, M. Fialho, T.C. Esteves, N.F. Santos, N. Ben Sedrine, L. Rino, A.J. Neves, K. Lorenz, E. Alves, T. Monteiro, Spectroscopic analysis of the NIR emission in Tm implanted $Al_xGa_{1-x}N$ layers, J. Appl. Phys. 120 (2016) 081701. doi:10.1063/1.4961931.

[19] E. Calleja, F.J. Sánchez, D. Basak, M.A. Sánchez-García, E. Muñoz, I. Izpura, F. Calle, J.M.G. Tijero, J.L. Sánchez-Rojas, B. Beaumont, P. Lorenzini, P. Gibart, Yellow luminescence and related deep states in undoped GaN, Phys. Rev. B. 55 (1997) 4689–4694. doi:10.1103/PhysRevB.55.4689.

[20] I. Shalish, L. Kronik, G. Segal, Y. Rosenwaks, Y. Shapira, U. Tisch, J. Salzman, Yellow luminescence and related deep levels in unintentionally doped GaN films, Phys. Rev. B. 59 (1999) 9748–9751. doi:10.1103/PhysRevB.59.9748.

[21] M.A. Reshchikov, H. Morkoç, Luminescence properties of defects in GaN, J. Appl. Phys. 97 (2005) 061301-061301-95. doi:doi:10.1063/1.1868059.

[22] T. Schulz, M. Albrecht, K. Irmscher, C. Hartmann, J. Wollweber, R. Fornari, Ultraviolet luminescence in AlN, Phys. Status Solidi B. 248 (2011) 1513–1518. doi:10.1002/pssb.201046616.

[23] E. Alves, K. Lorenz, R. Vianden, C. Boemare, M.J. Soares, T. Monteiro, Optical Doping of Nitrides by Ion Implantation, Mod. Phys. Lett. B. 15 (2001) 1281–1287. doi:10.1142/S0217984901003172.

[24] D.N. Faye, E. Wendler, M. Felizardo, S. Magalhães, E. Alves, F. Brunner, M. Weyers, K. Lorenz, Mechanisms of Implantation Damage Formation in $Al_xGa_{1-x}N$ Compounds, J. Phys. Chem. C. 120 (2016) 7277–7283. doi:10.1021/acs.jpcc.6b00133.

[25] P. Ruterana, M.-P. Chauvat, K. Lorenz, Mechanisms of Damage Formation during Rare Earth Ion Implantation in Nitride Semiconductors, Jpn. J. Appl. Phys. 52 (2013) 11NH02. doi:10.7567/JJAP.52.11NH02.

[26] K. Lorenz, E. Alves, I.S. Roqan, R.W. Martin, C. Trager-Cowan, K.P. O'Donnell, I.M. Watson, Rare earth doping of III-nitride alloys by ion implantation, Phys. Status Solidi A. 205 (2008) 34–37. doi:10.1002/pssa.200776714.

[27] K. Lorenz, U. Wahl, E. Alves, E. Nogales, S. Dalmasso, R.W. Martin, K.P. O'Donnell, M. Wojdak, A. Braud, T. Monteiro, T. Wojtowicz, P. Ruterana, S. Ruffenach, O. Briot, High temperature annealing of rare earth implanted GaN films: Structural and optical properties, Opt. Mater. (Amst). 28 (2006) 750–758. doi:10.1016/j.optmat.2005.09.015.

[28] J. Rodrigues, S.M.C. Miranda, A.J.S. Fernandes, E. Nogales, L.C. Alves, E. Alves, G. Tourbot, T. Auzelle, B. Daudin, B. Méndez, T. Trindade, K. Lorenz, F.M. Costa, T. Monteiro, Towards the understanding of the intentionally induced yellow luminescence in GaN nanowires, Phys. Status Solidi C. 10 (2013) 667–672. doi:10.1002/pssc.201200714.

[29] J. Rodrigues, M. Fialho, S. Magalhães, M.R. Correia, L. Rino, E. Alves, A.J. Neves, K. Lorenz, T. Monteiro, Analysis of the Tb^{3+} recombination in ion implanted $Al_xGa_{1-x}N$ ($0 \leq x \leq 1$) layers, J. Lumin. 178 (2016) 249–258. doi:10.1016/j.jlumin.2016.05.018.

[30] D. Chen, J. Wang, D. Xu, Y. Zhang, The influence of defects and impurities in polycrystalline AlN films on the violet and blue photoluminescence, Vacuum. 83 (2009) 865–868. doi:10.1016/j.vacuum.2008.09.003.

[31] B. Berzina, L. Trinkler, J. Grabis, I. Steins, Photoluminescence in AlN: macro-size and nano-powder, Phys. Status Solidi C. 4 (2007) 959–962. doi:10.1002/pssc.200673873.

[32] M. Peres, S. Magalhães, V. Fellmann, B. Daudin, A. Neves, E. Alves, K. Lorenz, T. Monteiro, Effect of Eu-implantation and annealing on the GaN quantum dots excitonic recombination, Nanoscale Res. Lett. 6 (2011) 378. doi:10.1186/1556-276X-6-378.

[33] B.G. Wybourne, Spectroscopic properties of rare earths, Interscience Publishers, Jonh Wiley & Sons Inc., New York, London , Sydney, 1965.

[34] T. Schmidt, K. Lischka, W. Zulehner, Excitation-power dependence of the near-band-edge photoluminescence of semiconductors, Phys. Rev. B. 45 (1992) 8989–8994. doi:10.1103/PhysRevB.45.8989.

[35] P.Y. Yu, M. Cardona, Fundamentals of Semiconductors: Physics And Materials Properties, Volume 3, Springer, 2005.

[36] J.I. Pankove, Optical Processes in Semiconductors, Dover Publication, Inc., 1971.

[37] T. Ogino, M. Aoki, Mechanism of Yellow Luminescence in GaN, Jpn. J. Appl. Phys. 19 (1980) 2395–2405. doi:10.1143/JJAP.19.2395.

[38] J. Neugebauer, C.G. Van de Walle, Gallium vacancies and the yellow luminescence in GaN, Appl. Phys. Lett. 69 (1996) 503. doi:10.1063/1.117767.

[39] R. Seitz, C. Gaspar, T. Monteiro, E. Pereira, M. Leroux, B. Beaumont, P. Gibart, Temperature behaviour of the yellow emission in GaN, MRS Int. J. Nitride Semicond. Res. 2 (1997) e36. doi:10.1557/S1092578300001629.

[40] M.A. Reshchikov, H. Morkoç, S.S. Park, K.Y. Lee, Transient photoluminescence of defect transitions in freestanding GaN, Appl. Phys. Lett. 78 (2001) 2882. doi:10.1063/1.1370119.

[41] M.A. Reshchikov, H. Morkoç, S.S. Park, K.Y. Lee, Two charge states of dominant acceptor in unintentionally doped GaN: Evidence from

photoluminescence study, Appl. Phys. Lett. 81 (2002) 4970. doi:10.1063/1.1531227.

[42] V. Darakchieva, T. Monteiro, J. Rodrigues, M.T. Son, M.-Y. Xie, N. Ben Sedrine, E. Alves, A. Usui, C. Hemmingson, B. Monemar, Electron irradiationof bulk HVPE GaN: structural properties and photoluminescence, in: Oral Present., ICNS-9, 2011.

[43] A. Sedhain, J. Li, J.Y. Lin, H.X. Jiang, Nature of deep center emissions in GaN, Appl. Phys. Lett. 96 (2010) 151902. doi:10.1063/1.3389497.

[44] M.A. Reshchikov, J.D. McNamara, H. Helava, A. Usikov, Y. Makarov, Two yellow luminescence bands in undoped GaN, Sci. Rep. 8 (2018) 8091. doi:10.1038/s41598-018-26354-z.

[45] J.L. Lyons, A. Janotti, C.G. Van de Walle, Carbon impurities and the yellow luminescence in GaN, Appl. Phys. Lett. 97 (2010) 152108. doi:10.1063/1.3492841.

[46] J.L. Lyons, A. Janotti, C.G. Van de Walle, Effects of carbon on the electrical and optical properties of InN, GaN, and AlN, Phys. Rev. B. 89 (2014) 035204. doi:10.1103/PhysRevB.89.035204.

[47] M.A. Reshchikov, D.O. Demchenko, A. Usikov, H. Helava, Y. Makarov, Carbon defects as sources of the green and yellow luminescence bands in undoped GaN, Phys. Rev. B. 90 (2014) 235203. doi:10.1103/PhysRevB.90.235203.

[48] M.A. Reshchikov, N.M. Albarakati, M. Monavarian, V. Avrutin, H. Morkoç, Thermal quenching of the yellow luminescence in GaN, J. Appl. Phys. 123 (2018) 161520. doi:10.1063/1.4995275.

[49] Y. Ohba, H. Yoshida, R. Sato, Growth of High-Quality AlN, GaN and AlGaN with Atomically Smooth Surfaces on Sapphire Substrates, Jpn. J. Appl. Phys. 36 (1997) L1565–L1567. doi:10.1143/JJAP.36.L1565.

[50] B. Liu, R. Zhang, Z.L. Xie, Q.J. Liu, Z. Zhang, Y. Li, X.Q. Xiu, J. Yao, Q. Mei, H. Zhao, P. Han, H. Lu, P. Chen, S.L. Gu, Y. Shi, Y.D. Zheng, W.Y. Cheung, N. Ke, J.B. Xu, Al incorporation, structural and optical properties of $Al_xGa_{1-x}N$ ($0.13 \leqslant x \leqslant 0.8$) alloys grown by MOCVD, J. Cryst. Growth. 310 (2008) 4499–4502. doi:10.1016/J.JCRYSGRO.2008.07.076.

[51] A. Wakahara, Y. Nakanishi, T. Fujiwara, A. Yoshida, T. Ohshima, T. Kamiya, Enhancement effect of Tb-related luminescence in $Al_xGa_{1-x}N$ with the AlN molar fraction 0≤x≤1, Phys. Status Solidi A. 202 (2005) 863–867. doi:10.1002/pssa.200461430.

[52] H.J. Lozykowski, W.M. Jadwisienczak, I. Brown, Photoluminescence and cathodoluminescence of GaN doped with Tb, Appl. Phys. Lett. 76 (2000) 861. doi:10.1063/1.125609.

[53] W.M. Jadwisienczak, H.J. Lozykowski, F. Perjeru, H. Chen, M. Kordesch, I.G. Brown, Luminescence of Tb ions implanted into amorphous AlN thin films grown by sputtering, Appl. Phys. Lett. 76 (2000) 3376. doi:10.1063/1.126652.

[54] M. Inokuti, F. Hirayama, Influence of Energy Transfer by the Exchange Mechanism on Donor Luminescence, J. Chem. Phys. 43 (1965) 1978. doi:10.1063/1.1697063.

[55] A. Bell, Exciton freeze-out and thermally activated relaxation at local potential fluctuations in thick $Al_xGa_{1-x}N$ layers, J. Appl. Phys. 95 (2004) 4670. doi:10.1063/1.1689736.

[56] Y.-H. Cho, G.H. Gainer, J.B. Lam, J.J. Song, W. Yang, W. Jhe, Dynamics of anomalous optical transitions in $Al_xGa_{1-x}N$ alloys, Phys. Rev. B. 61 (2000) 7203–7206. doi:10.1103/PhysRevB.61.7203.

[57] T.Y. Lin, J.C. Fan, Y.F. Chen, Effects of alloy potential fluctuations in InGaN epitaxial films, Semicond. Sci. Technol. 14 (1999) 406–411. doi:10.1088/0268-1242/14/5/006.

[58] G. Steude, B.K. Meyer, A. Göldner, A. Hoffmann, F. Bertram, J. Christen, H. Amano, I. Akasaki, Optical investigations of AlGaN on GaN epitaxial films, Appl. Phys. Lett. 74 (1999) 2456. doi:10.1063/1.123879.

[59] S.J. Chung, M.S. Kumar, H.J. Lee, E.-K. Suh, Investigations on alloy potential fluctuations in epilayers using optical characterizations, J. Appl. Phys. 95 (2004) 3565–3568. https://doi.org/10.1063/1.1652256.

[60] E. Kuokstis, W.H. Sun, M. Shatalov, J.W. Yang, M.A. Khan, Role of alloy fluctuations in photoluminescence dynamics of AlGaN epilayers, Appl. Phys. Lett. 88 (2006) 261905–62103. doi:10.1063/1.1689736.

[61] K. Kazlauskas, A. Žukauskas, G. Tamulaitis, J. Mickevičius, M.S. Shur, R.S. Qhalid Fareed, J.P. Zhang, R. Gaska, Exciton hopping and nonradiative decay in AlGaN epilayers, Appl. Phys. Lett. 87 (2005) 172102–62103. doi:10.1063/1.2112169.

[62] A. Redondo-Cubero, K. Lorenz, E. Wendler, D. Carvalho, T. Ben, F.M. Morales, R. García, V. Fellmann, B. Daudin, Selective ion-induced intermixing and damage in low-dimensional GaN/AlN quantum structures., Nanotechnology. 24 (2013) 505717. doi:10.1088/0957-4484/24/50/505717.

[63] H. Shibata, Negative Thermal Quenching Curves in Photoluminescence of Solids, Jpn. J. Appl. Phys. 37 (1998) 550–553. doi:10.1143/JJAP.37.550.

[64] Y. Wu, J. Li, H. Ding, Z. Gao, Y. Wu, N. Pan, X. Wang, Negative thermal quenching of photoluminescence in annealed ZnO–Al_2O_3 core–shell nanorods, Phys. Chem. Chem. Phys. 17 (2015) 5360–5365. doi:10.1039/C4CP04998E.

[65] S.S. Lin, B.G. Chen, W. Xiong, Y. Yang, H.P. He, J. Luo, Negative thermal quenching of photoluminescence in zinc oxide nanowire-core/graphene-shell complexes, Opt. Express. 20 (2012) A706. doi:10.1364/OE.20.00A706.

[66] Y. Nakanishi, A. Wakahara, H. Okada, A. Yoshida, T. Ohshima, H. Itoh, Improvement of luminescence capability of Tb^{3+}-related emission by $Al_xGa_{1-x}N$, Phys. Status Solidi. 240 (2003) 372–375. doi:10.1002/pssb.200303479.

[67] H. Lozykowski, Kinetics of luminescence of isoelectronic rare-earth ions in III-V semiconductors, Phys. Rev. B. 48 (1993) 17758–17769. doi:10.1103/PhysRevB.48.17758.

[68] H.J. Lozykowski, W.M. Jadwisienczak, Thermal quenching of luminescence and isovalent trap model for rare-earth-ion-doped AlN, Phys. Status Solidi. 244 (2007) 2109–2126. doi:10.1002/pssb.200642152.

[69] H.J. Lozykowski, W.M. Jadwisienczak, I. Brown, Photoluminescence and cathodoluminescence of GaN doped with Pr, J. Appl. Phys. 88 (2000) 210. doi:10.1063/1.373645.

[70] W.M. Jadwisienczak, The Luminescence Properties of the Wide Bandgap Nitrides Doped with Rare Earth ions and Gallium Nitride Doped with Conventional Isoelectronic Impurities, Ohio University, 2001.

[71] H. Angerer, D. Brunner, F. Freudenberg, O. Ambacher, M. Stutzmann, R. Höpler, T. Metzger, E. Born, G. Dollinger, A. Bergmaier, S. Karsch, H.-J. Körner, Determination of the Al mole fraction and the band gap bowing of epitaxial $Al_xGa_{1-x}N$ films, Appl. Phys. Lett. 71 (1998) 1504. doi:10.1063/1.119949.

[72] P. Dorenbos, E. van der Kolk, Location of lanthanide impurity energy levels in the III–V semiconductor $Al_xGa_{1-x}N$ ($0 \leqslant x \leqslant 1$), Opt. Mater. (Amst). 30 (2008) 1052–1057. doi:10.1016/j.optmat.2007.05.019.

[73] P. Dorenbos, E. van der Kolk, Lanthanide impurity level location in GaN, AlN, and ZnO, in: H. Morkoc, C.W. Litton (Eds.), Proc. SPIE 6473, Gall. Nitride Mater. Devices II, International Society for Optics and Photonics, 2007: pp. 647313-647313–10. doi:10.1117/12.698977.

[74] P. Dorenbos, Systematic behaviour in trivalent lanthanide charge transfer energies, J. Phys. Condens. Matter. 15 (2003) 8417–8434. doi:10.1088/0953-8984/15/49/018.

[75] P. Dorenbos, E. Van der Kolk, Location of lanthanide impurity levels in the III-V semiconductor GaN, Appl. Phys. Lett. 89 (2006) 061122. doi:https://doi.org/10.1063/1.2336716.

[76] P. Dorenbos, Locating lanthanide impurity levels in the forbidden band of host crystals, J. Lumin. 108 (2004) 301–305. doi.org/10.1016/j.jlumin.2004.01.064.

Figure caption

Figure 1 – (a) 14 K PL spectra of the $Al_{0.2}Ga_{0.8}N$ samples implanted at different temperatures (post-implantation annealing at 1200 ºC). (b) High-resolution PL spectrum of the Tb^{3+} emission lines for the sample implanted at 550 ºC, evidencing the ion multiplet splitting.

Figure 2 – Log (I/I_0)-log (P/P_0) plot for the visible broad band of the samples implanted at (a) 140 ℃ and (b) 300 ℃, after Gaussian fit of the visible PL band.

Figure 3 – RT time-resolved PL of the visible broad band of the samples implanted at (a) 140 ℃ and (b) 300 ℃, using a sample window of 10 ms for different time delays.

Figure 4 – Temperature dependence of the PL emission in the UV-Vis range for $Al_{0.2}Ga_{0.8}N$:Tb samples implanted at (a) RT, (b) 140 ℃, (c) 3 00 ℃ and (d) 550 ℃.

Figure 5 – Peak position *vs* temperature for the yellow band of the $Al_{0.2}Ga_{0.8}N$:Tb samples implanted at (a) RT, (b) 140 ℃, (c) 300 ℃ and (d) 550 ℃.

Figure 6 – Integrated intensity of the visible band as a function of temperature, obtained after the Gaussian fit used to calculate the integrated intensity of the defect emission, for samples implanted at (a) RT, (b) 140 ℃, (c) 300 ℃ and (d) 550 ℃. The red line denotes the fitting of the experimental results using Eq. (1).

Figure 7 – Temperature dependent PL of the $^5D_4 \rightarrow {}^7F_6$ transition after the baseline removal (obtained from the fitting of the yellow band) for the $Al_{0.2}Ga_{0.8}N$:Tb samples implanted at (a) RT, (b) 140 ℃, (c) 300 ℃ and (d) 550 ℃.

Figure 8 – Integrated intensity of the $^5D_4 \rightarrow {}^7F_6$ transition as a function of temperature (obtained from the data represented in Figure 7) for samples implanted at (a) RT, (b) 140 ℃, (c) 300 ℃ and (d) 550 ℃. The red line den otes the fitting of the experimental results using Eq. (2).

Figure 9 – (a) RT PLE spectra for the $Al_{0.2}Ga_{0.8}N$:Tb samples. The spectra are ordered from the sample with highest (140 ºC) to the one with the lowest (300 ºC) damage concentration, including also the spectra for the as-grown samples (bottom). (b) RT PL spectra of the $Al_{0.2}Ga_{0.8}N$ sample implanted at 300 ºC excited with different wavelengths.

Figure 1

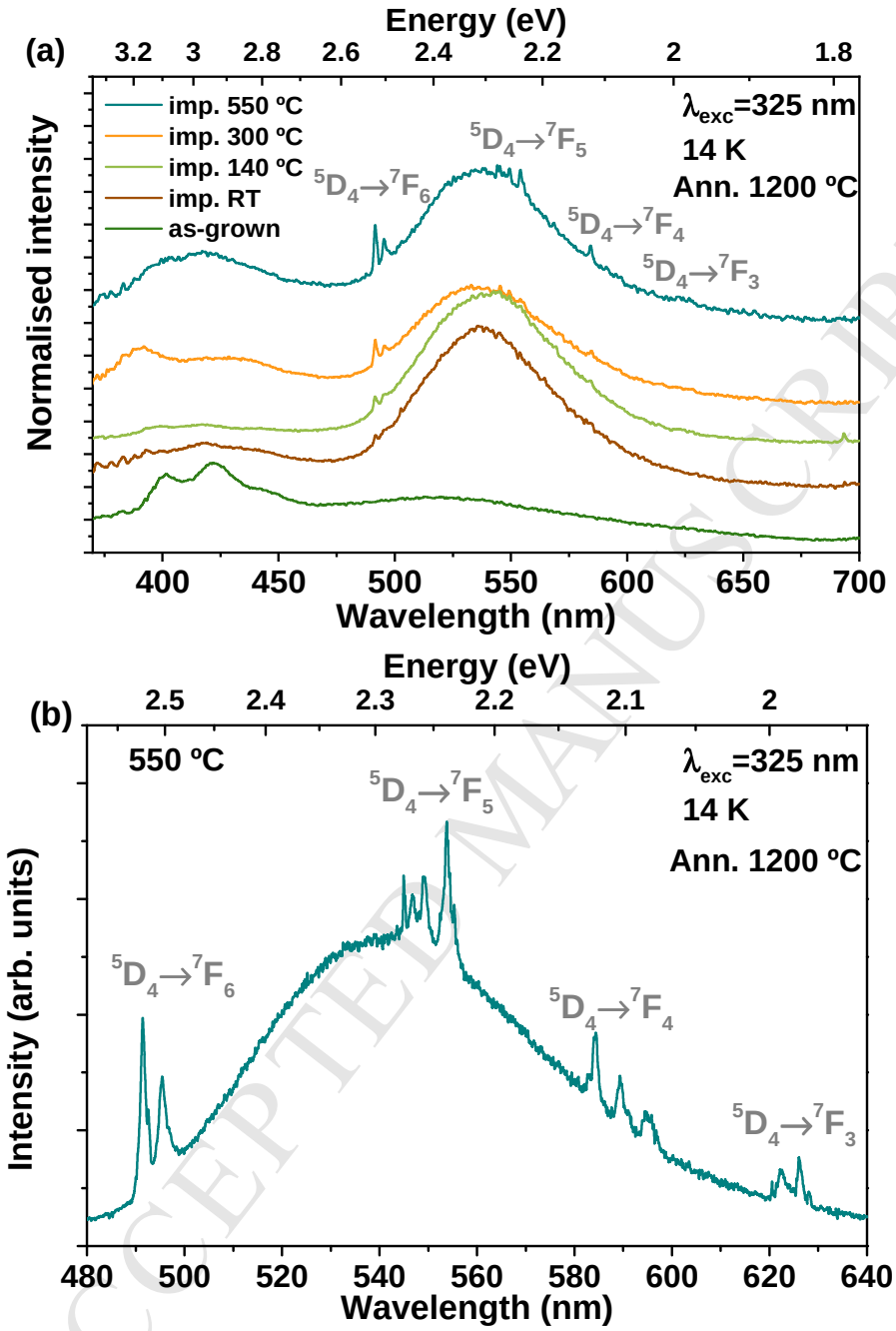

Figure 2

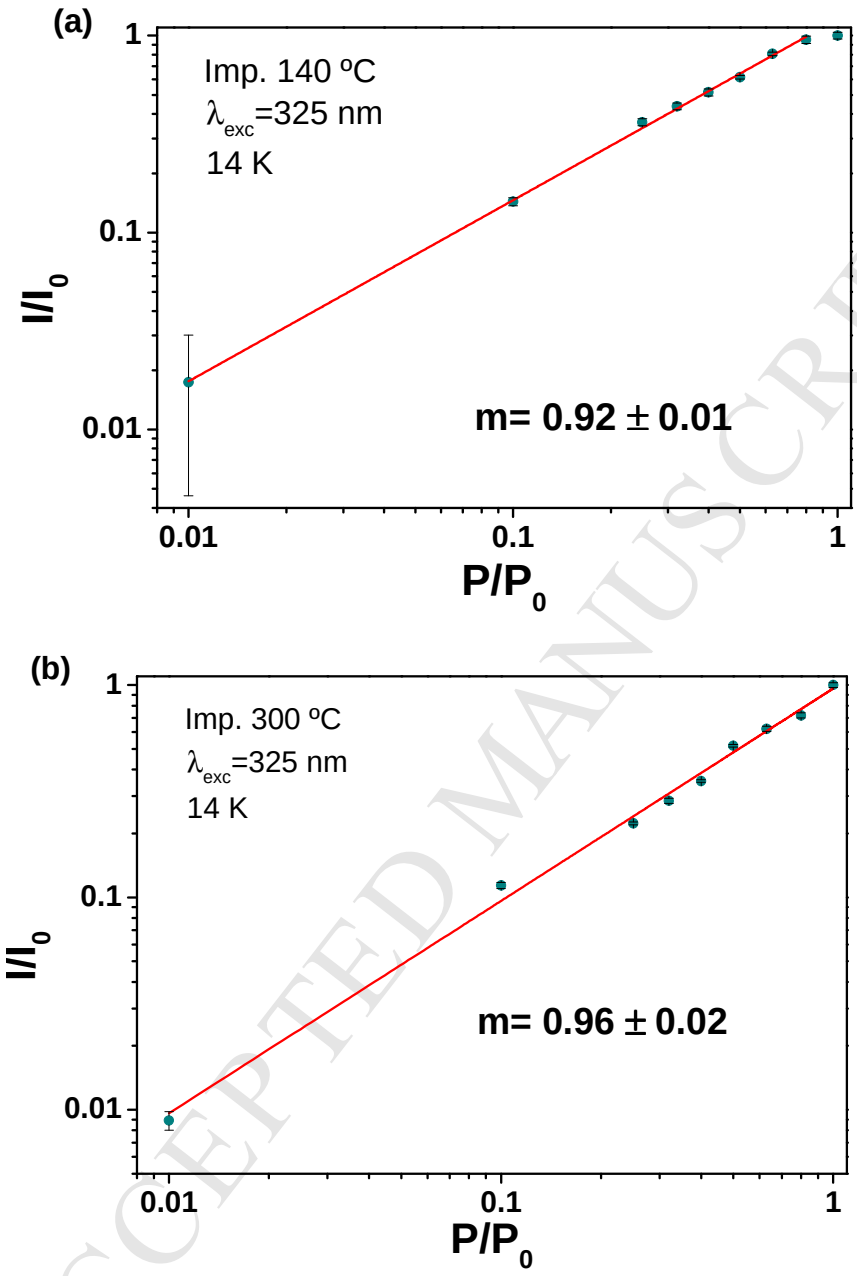

Figure 3

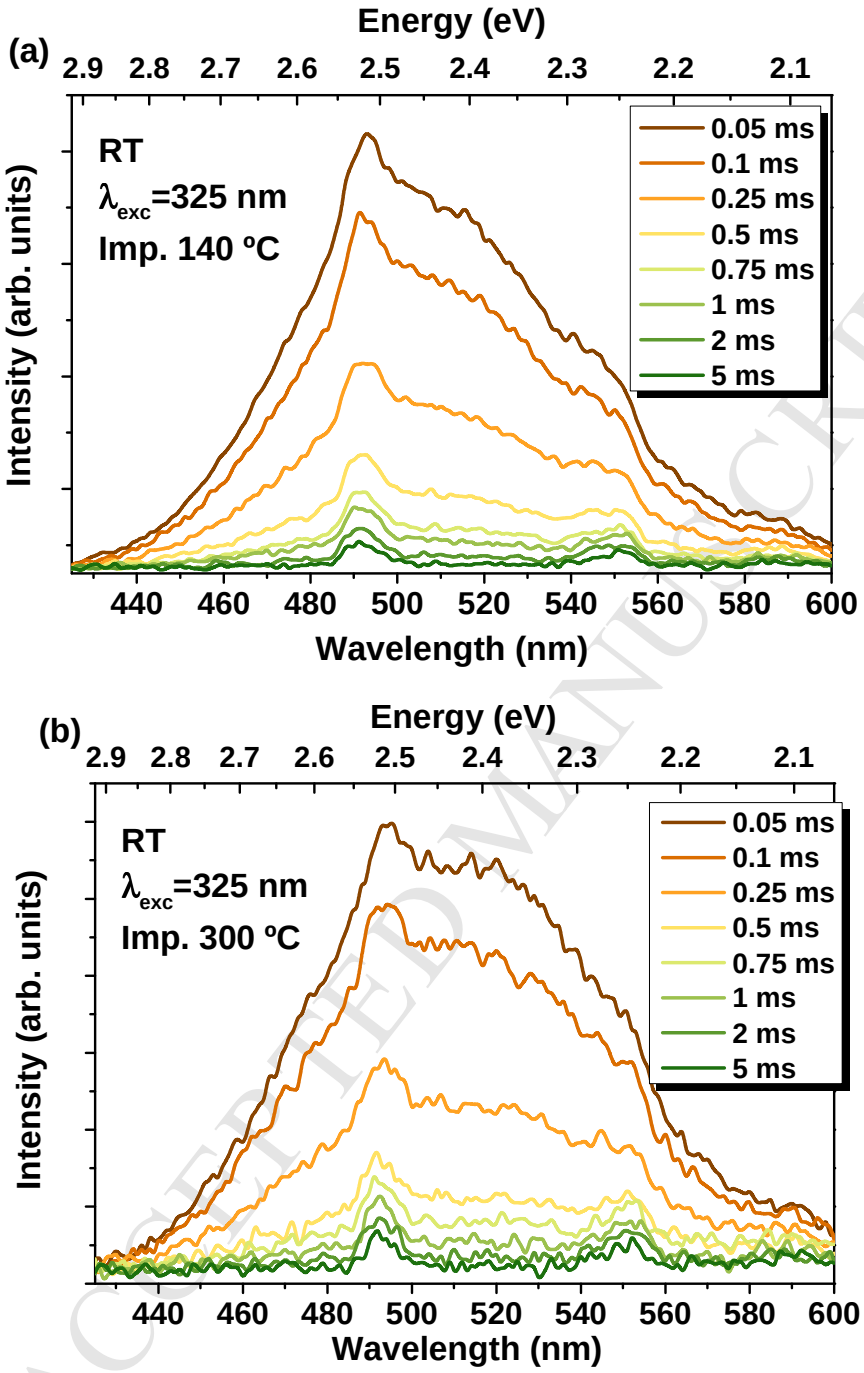

Figure 4

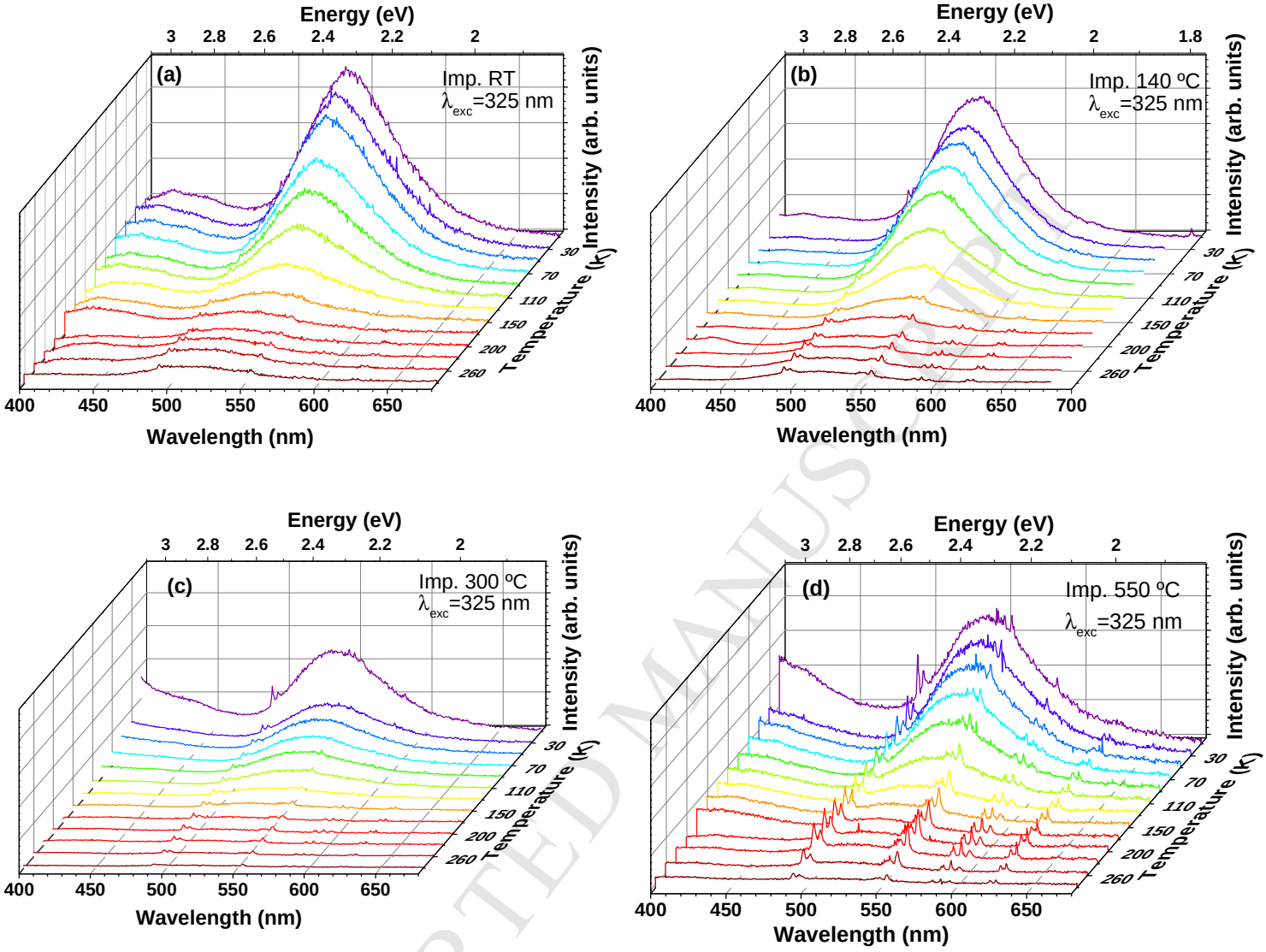

Figure 5

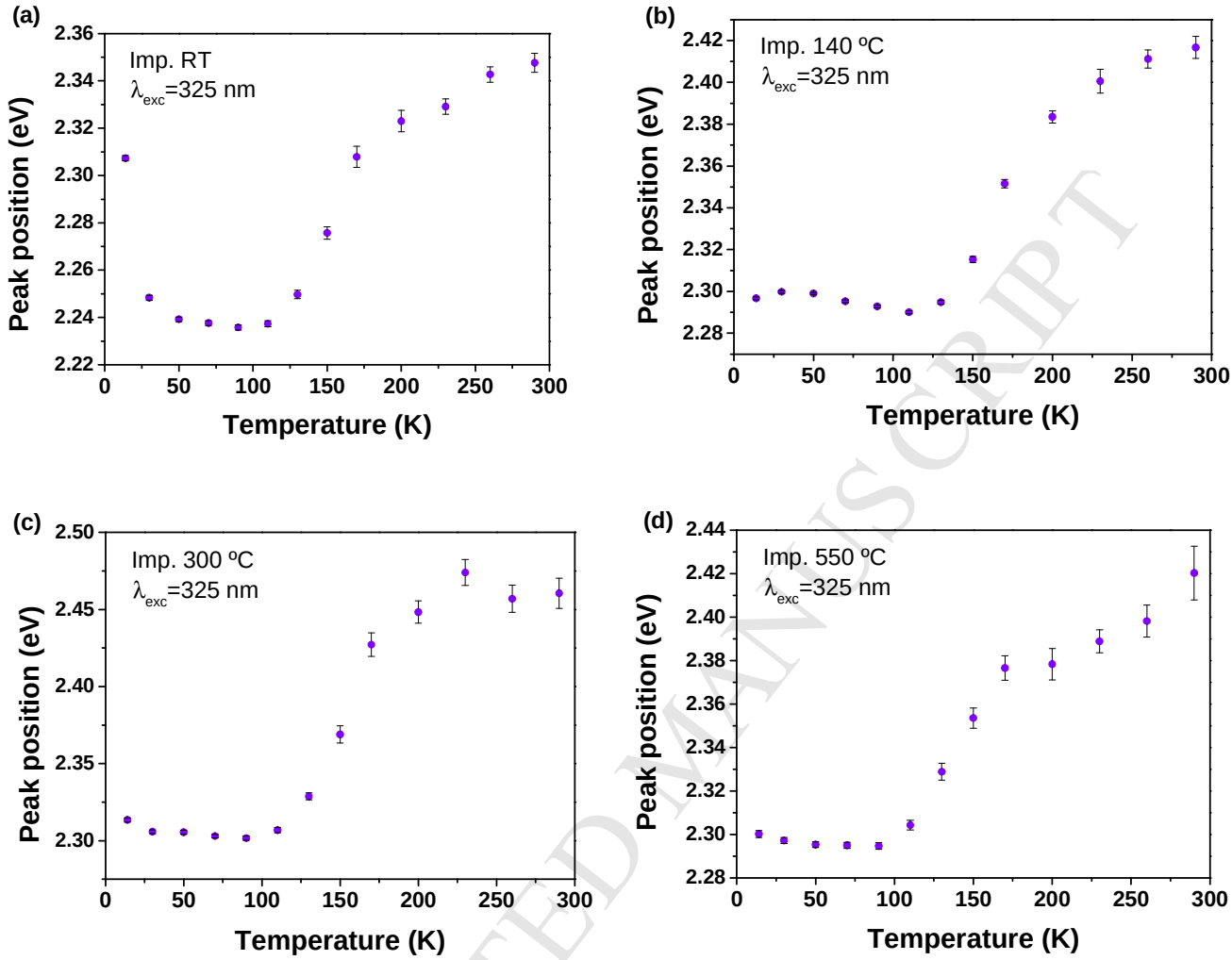

Figure 6

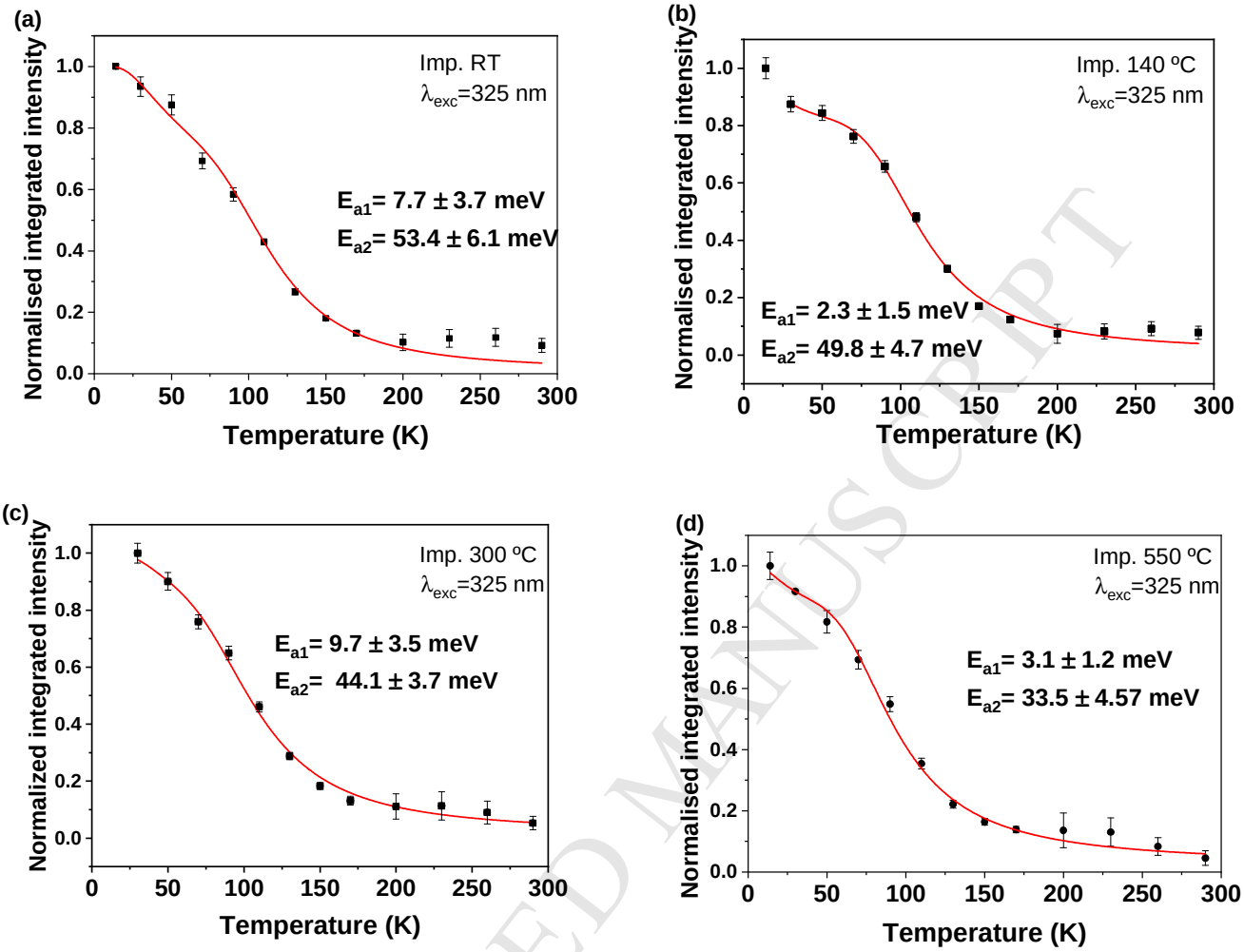

Figure 7

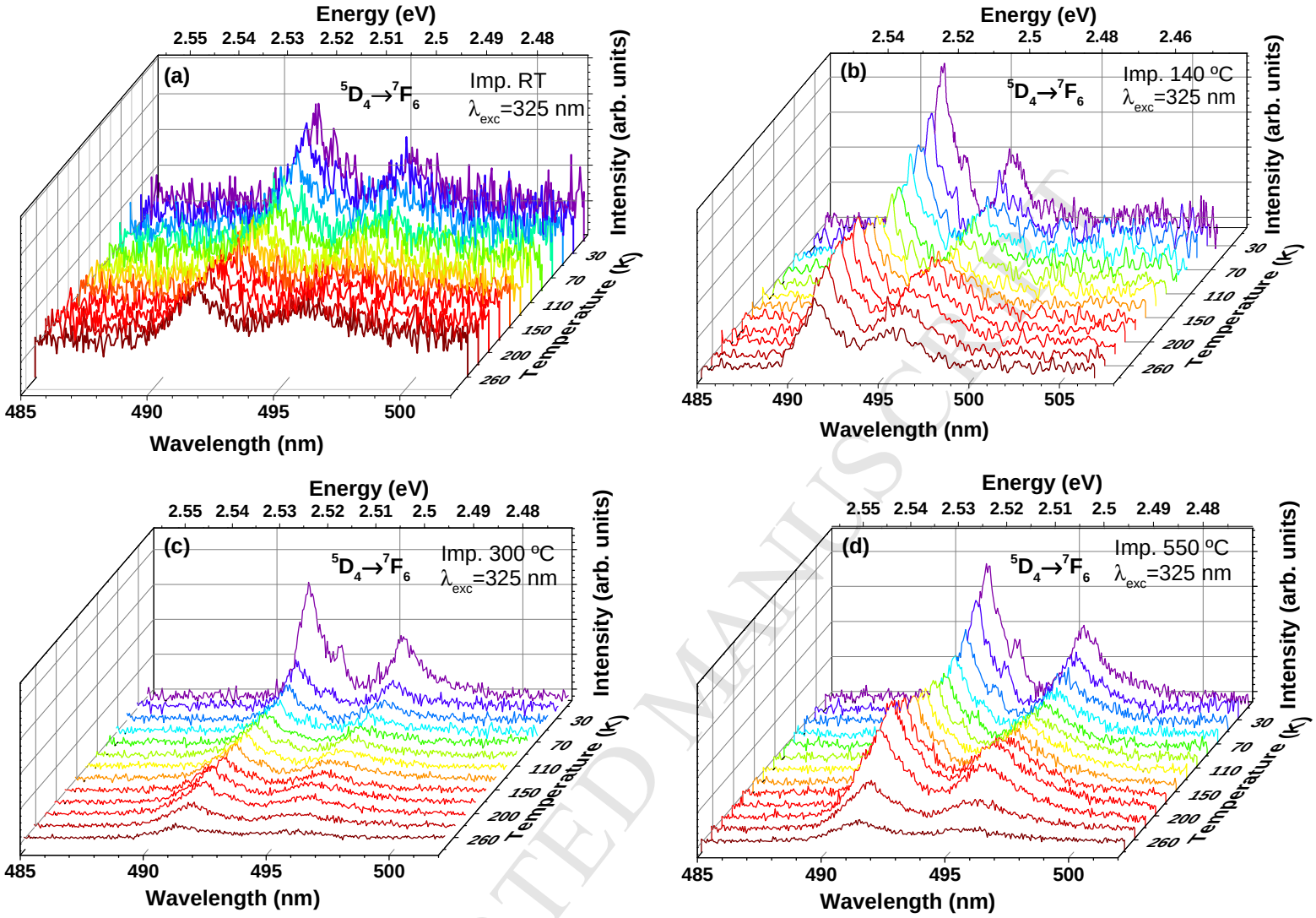

Figure 8

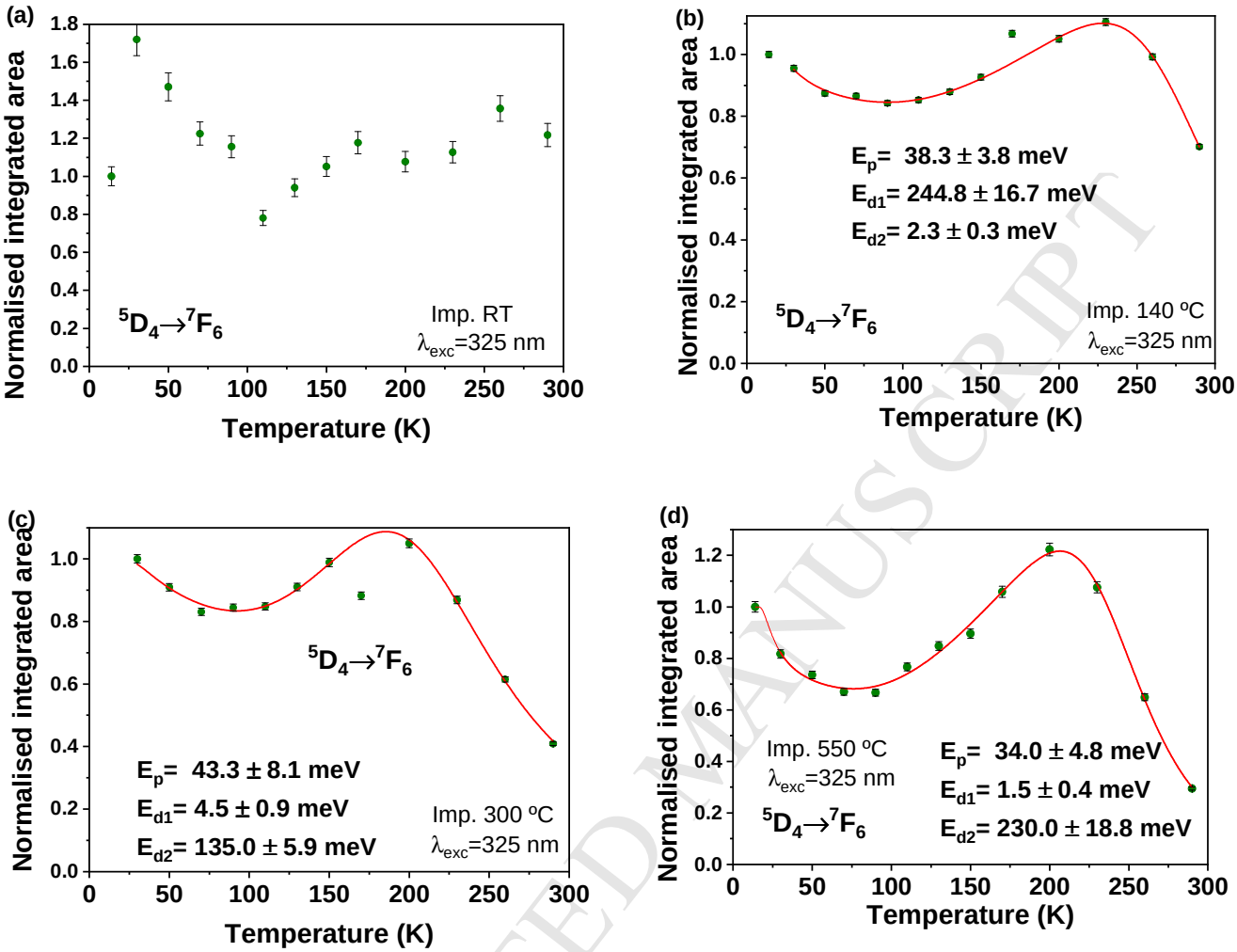

Figure 9